*Reprinted from*

JAPANESE JOURNAL OF
APPLIED
PHYSICS

**REGULAR PAPER**

# Optimization of Seesaw Swing Arm Actuator Design for Small Form Factor Optical Disk Drive

Po-Chien Chou, Yu-Cheng Lin, and Stone Cheng

Jpn. J. Appl. Phys. **49** (2010) 052502

© 2010 The Japan Society of Applied Physics

Person-to-person distribution (up to 10 persons) by the author only. Not permitted for publication for institutional repositories or on personal Web sites.

Japanese Journal of Applied Physics **49** (2010) 052502 **REGULAR PAPER**

# Optimization of Seesaw Swing Arm Actuator Design for Small Form Factor Optical Disk Drive

Po-Chien Chou, Yu-Cheng Lin, and Stone Cheng*

*Department of Mechanical Engineering, National Chiao Tung University, Hsinchu 300, Taiwan*

Received December 3, 2009; accepted January 21, 2010; published online May 20, 2010

Many small form factor (SFF) optical pickup heads based on the swing arm design utilize a piezoelectric material or the slim metal plate to perform the focusing action. The seesaw-type actuator is a new mechanism used in the focusing action for SFF optical data storage devices. The swing arm nutates along a pivot instead of a hinge in the vertical movement. In this paper, an optimized design of a biaxial voice coil motor (VCM), in which the tracking and focusing VCMs are combined in the rear of the swing arm, is proposed. Simulation and experiment results demonstrate the effectiveness of the proposed design methodology by showing that the stress magnitude distribution characteristics, mechanism stiffness, and driving stability of the optimized design are enhanced in comparison with those of the original. © 2010 The Japan Society of Applied Physics

DOI: 10.1143/JJAP.49.052502

## 1. Introduction

Optical disk drives are one of the most popular systems for information storage. Obtaining the required high track density and accurate focusing requires a high-precision servo system. The micro-optical disk drive (ODD) can be a solution for compact size and portability. The development of a micro-optical head with a swing arm actuator is significant for new optical storage technology. Rather than a mechanism design of a swing arm, most research work has focused on the micro-optical system design required to provide the optical characteristics. A swing-arm-type rotary actuator has advantages over a linear actuator in terms of fast access time, slim shape, mobility, and high mechanical performance.

Several papers on slider design or improvements of ODD systems have been introduced.[1,2] However, the important mechanical issues regarding the design of the suspension, swing arm, and the air gap between the magnets and yoke have not been discussed in the literature. In this paper, a new design that uses a biaxial voice coil motor (VCM) and multi segmented magnet arrays (MSMA) with numerical simulations are presented to evaluate the electromagnetic performance. We designed a seesaw mechanism of a rotary type miniaturized actuator with a focusing mechanism with sufficient mechanical bandwidth for a micro-ODD.[3,4] In DataPlay's patents and other typical focusing mechanism designs, a hinged plate with a coil mounted for focusing is controlled by a VCM driver. However, the thin metal hinge is weak and tends to fracture with repeated operations.[5] To resolve this problem, the proposed design replaces the hinge spring with a seesaw movement. The initial seesaw actuator was designed on the basis of electromagnetic (EM) and structural analyses for both focusing and tracking actuators. Each mechanical part is designed to satisfy the requirements of the servo control performance and dynamic characteristics.[6,7] To maximize the seesaw actuator driving force, a magnetic circuit with a fan-shaped magnet was suggested for the voice coil motion. A combination of three fan-shaped magnets and a ring tracking yoke was used in the actuator magnetic circuit. The new mechanism was also optimized to obtain high seesaw arm stiffness and improved swinging performance within the mechanical tolerances using the proposed design procedure based on finite element (FE) and EM analyses. To estimate the swing stability of the optimum design, the dynamic characteristics of seesaw swing mechanism were also investigated.[8,9]

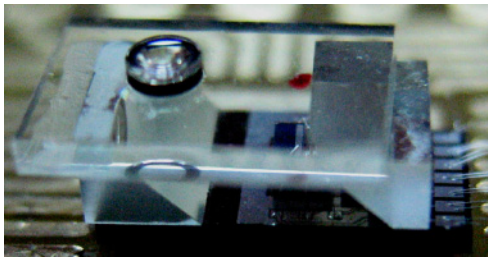

(a)

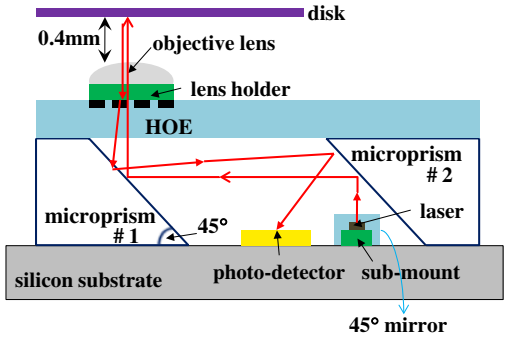


(b)

**Fig. 1.** (Color online) Schematic diagram of the optical head (the laser is bounded on a submount and emitting light from the direction into the paper): (a) schematic diagram of the micro-optical configuration, and (b) schematic diagram of the small form factor optical configuration.

## 2. Micro-optical Pickup Head Configuration

The optical head combined with a seesaw swing arm actuator and an optical module is designed for small form factor (SFF) drives. This system adopts a finite-conjugate objective lens with a numerical aperture (NA) of 0.65 for a 635 nm wavelength. Figure 1 shows the optical configuration based on the parameters in Table I. A laser chip is bonded on a submount with special metal coatings. The 45° turning mirror, micro-prism #2, reflects the laser beam upward 45°, and then another 45° mirror, micro prism #1, redirects the beam by another 45° so that it enters the holographic optical element (HOE) perpendicular, and the zero-order beam passes through the objective lens to focus on the disk. The returning beam is diffracted by the HOE and reflected by micro prism #1 to micro prism #2. Finally, the returning

*E-mail address: stonecheng@mail.nctu.edu.tw

 © 2010 The Japan Society of Applied Physics

Person-to-person distribution (up to 10 persons) by the author only. Not permitted for publication for institutional repositories or on personal Web sites.



**Table I.** Specifications of micro-optics pickup optical parameters.

| Item | Proposed system |
|---|---|
| Laser wavelength (nm) | 654 |
| Image-object relation | Finite-conjugate system |
| Focal length (mm) | 0.670 |
| Object NA (laser side) | 0.1 |
| Image NA (disk side) | 0.65 |
| Clear aperture diameter (mm) | 1.1 |

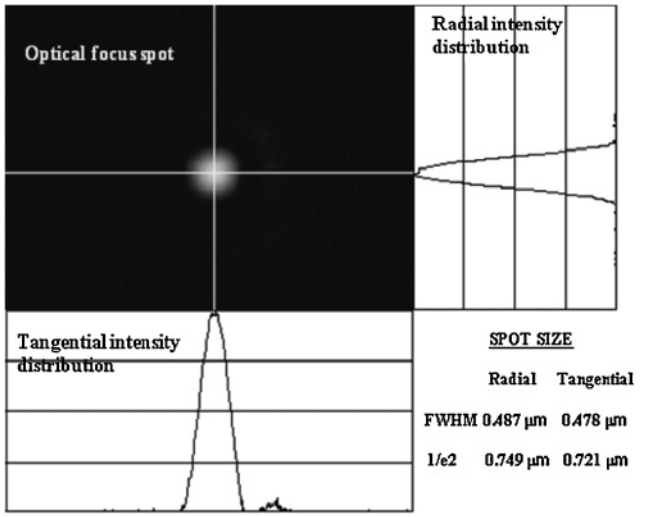


**Fig. 2.** Measurement of focused DVD laser spot in micro-optical pickup head.

beam arrives on the quadrant photo detector. Using an HOE efficiently simplifies the optical configuration and significantly reduces the number of components.[10] This optical construction can be applied to high-density blue-ray storage and holographic optical storage in SFFs in the immediate future.[11,12] We measured the focused laser spot of this micro-optical pickup system, as shown in Fig. 2. The spot intensity is normally distributed and has some slight aberration.

## 3. Initial Seesaw Type VCM Actuator Design and Simulation

Referring to Fig. 3, the optical disc system called "TOPY", which is developed by DataPlay, uses a swing arm type actuator. The fine tracking and coarse seeking are achieved with the single VCM shown at the end of the back suspension and cartridge pivot bearing. The tracking path follows the curved path of the swing arm rather than the straight line of a linear motor. Focusing motions are achieved with the voice coil motor shown at the center of the front suspension.[13] Several reports have described the use of a swing arm to realize a micro-storage system. To improve its material properties, triple layers of steel, aluminum and steel, form the swing arm structure.[14–16] However, this hinge structure gives the swing arm low stiffness. Furthermore, this stresses the hinges, which have limited elastic and plastic strain endurance. The hinge springs are too weak for repetitive operation and can fracture. Furthermore, the hinge spring rate and ballast weight affect the shock resistance of the suspension. To increase the swing arm actuator resonance frequency, three methods are commonly applied: (1)

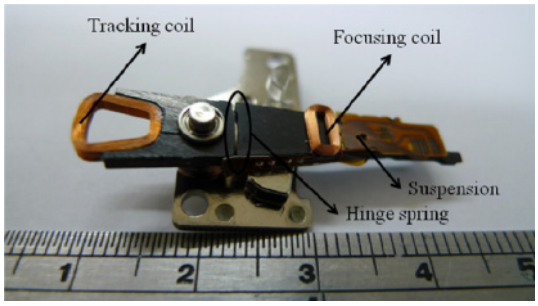


**Fig. 3.** (Color online) DataPlay's swing arm actuator.

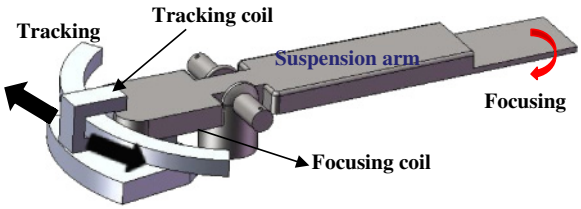


**Fig. 4.** (Color online) Tracking and focusing movement.

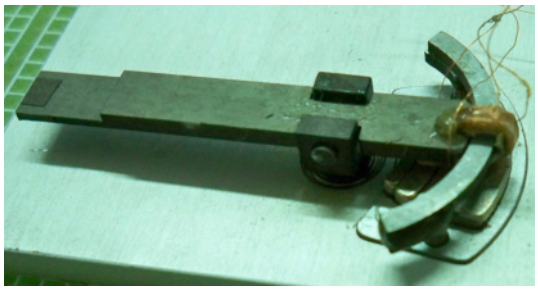

**Fig. 5.** (Color online) Fabricated "seesaw-shaped" VCM actuator.

using a high Young's-modulus-to-density ratio material, such as a titanium alloy; however, controlling or changing the material properties is not easy; (2) strengthening the load suspension stiffness with embossments to approach the shape optimization of the suspension; and (3) removing the high-kinetic-energy region of the mass.

As an improvement over the fragile hinge spring, a seesaw-type rotary VCM actuator without a hinge spring was suggested for the fine focusing motion. A schematic of this swing arm focusing concept is shown in Figs. 4 and 5. A seesaw is an accurate lever machine that magnifies force; it consists of a seesaw arm (lever arm) and pivot axial base (fulcrum). The seesaw arm was connected to two steel balls by fixed cylinder pins; the conical aperture of the cylinder pins restricted the ball rotation. The balls are designed specifically for rotating along one degree of freedom along the $X$-axis (in the direction of the pin clamp). The driving force creates a torque around the fulcrum, and this torque is dependent on the magnitude of the VCM driving force and the distance from the fulcrum to the focusing coil. When the driving force produces the moment around the axial base, the seesaw arm has a nutating motion along the focusing direction. In this case, as the focus ranges in the seesaw arm are equal to those of the hinge-type, the rotation angle in


© 2010 The Japan Society of Applied Physics

Person-to-person distribution (up to 10 persons) by the author only. Not permitted for publication for institutional repositories or on personal Web sites.



**Table II.** Five modal resonance characteristics.

| Mode | Resonance frequency (Hz) | Response mode |
|---|---|---|
| I | 38 | Cantilever |
| II | 1285.6 | First bending |
| III | 2531 | Second bending |
| IV | 5174 | First torsion |
| V | 7648 | Second torsion |

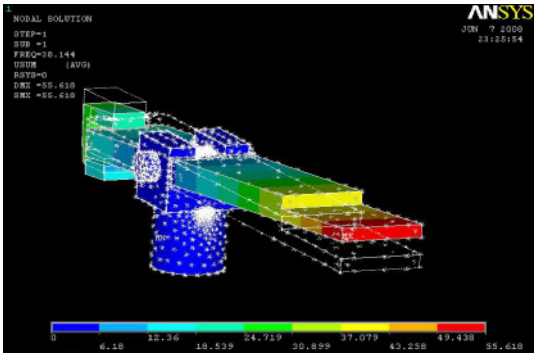


**Fig. 6.** (Color online) Mode I cantilever: 38 Hz.

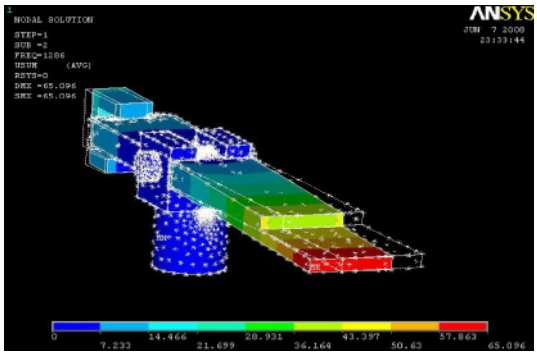


**Fig. 7.** (Color online) Mode II first bending: 1285.6 Hz.

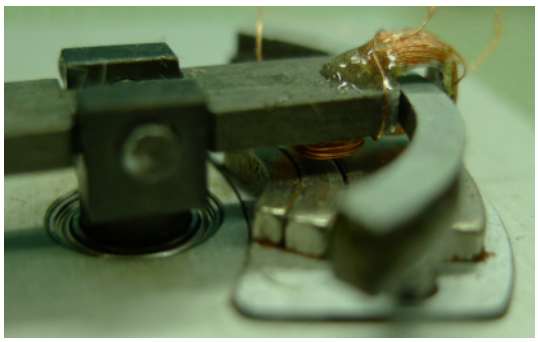

**Fig. 8.** (Color online) Lateral view of MSMA magnets.

new design is smaller because it's has larger turning radius. The seesaw actuator can be effectively reduce the angle of deviation and performs precise focusing motion for the seesaw actuator. The advantages of this initial design are that the moving parts weigh less than those of an actuator with a hinge spring, and a hinge spring connected to the suspension decreases lateral stiffness. To compensate for this weakness, we reinforce it with a material, such as an aluminum alloy of light metal, instead of the complex and expensive triple layers. Finally, the total length of the actuator can be minimized by adopting the seesaw shape. This actuator has excellent linearity within the movement range and is more effective than the hinge spring.

To improve the dynamic characteristics of the fabricated seesaw actuator, both the finite element model and EM simulation are conformed to the actual mechanical characteristics of the actuator system. System optimization is performed using the Computer-aided engineering (CAE) optimization tool in ANSYS using a total of 14,243 elements that have eight node bricks (SOLID). The seesaw arm is optimized to guarantee tracking and focusing stability. Six variables selected for the total seesaw shaped parameters are chosen as the design factors. The objectives are five resonance frequencies which are shown in Table II: cantilever, first and second bending, and first and second torsion modes. Figures 6 and 7 show the two mode shapes and characteristics of the seesaw arm; Fig. 6 shows the first cantilever mode frequency of 38 Hz in the focusing direction, and Fig. 7 shows the first bending mode frequency of 1285.6 Hz in the tracking direction.

In a typical VCM design, the magnet form is the coupled fan shape with S and N poles on the right and left sides, respectively. A conventional VCM uses only a vertically magnetized magnet, however, the new MSMA VCM contains both vertically ($Y$-direction) and horizontally ($X$-direction) magnetized magnets.[17,18] The principle is that the magnetic field is concentrated on one side while it is diminished on the other side if $X$-directional magnets are combined with the $Y$-directional magnet array. If the MSMA is used in an electric motor instead of a conventional magnet array, the coil is exposed to more magnetic flux. As shown in Fig. 8, we propose a three layer MSMA to reduce the out-of-plane force. The proposed design consists of a ring yoke, base yoke, and fan shaped magnets. This design has three special features for reducing out-of-plane force. First, the outer portion of the coil is separated from the edge of the MSMA magnets to decrease the force due to magnetic flux leaking from the edge. Second, the magnetic transition line of the magnet with a ring yoke is shorter than that in a conventional design, decreasing the out-of-plane force at the magnetic transition line; there are some concerns about driving torque reduction and increases in the mass of the coil and magnet. We achieved a VCM design with a small off-plane force at low cost. Third, the number of voice coil turns was estimated from the magnetic variables by considering the inevitable air gaps for avoiding contact between the yoke and the magnets. The ring yoke shortened the gap and effectively diminished the number of coil turns. Generally, if the VCM can generate a large force, the seesaw arm will be driven faster and be more robust against disturbances. Our aim is to design a VCM that can generate as much force as possible with a limited actuator size.[19]

The simulation results of the three-dimensional (3D) Maxwell EM model for the ring yoke and base yoke are shown in Figs. 9 and 10, respectively. The relationship between the dynamic characteristics of the actuator and the


© 2010 The Japan Society of Applied Physics

Person-to-person distribution (up to 10 persons) by the author only. Not permitted for publication for institutional repositories or on personal Web sites.



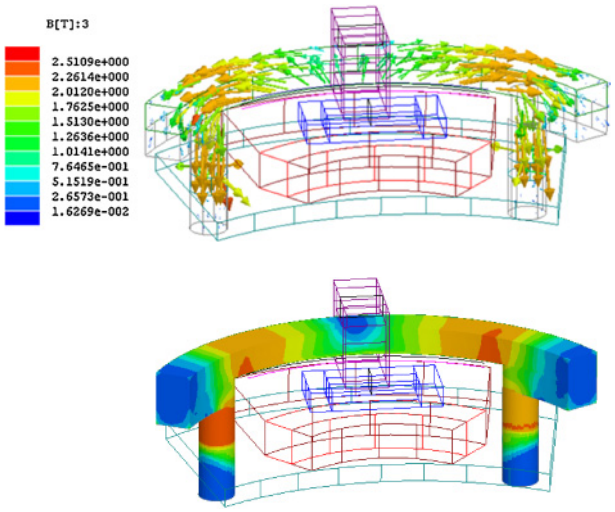


**Fig. 9.** (Color online) 3D EM model and magnetic flux lines on cross-sectional view of ring yoke.

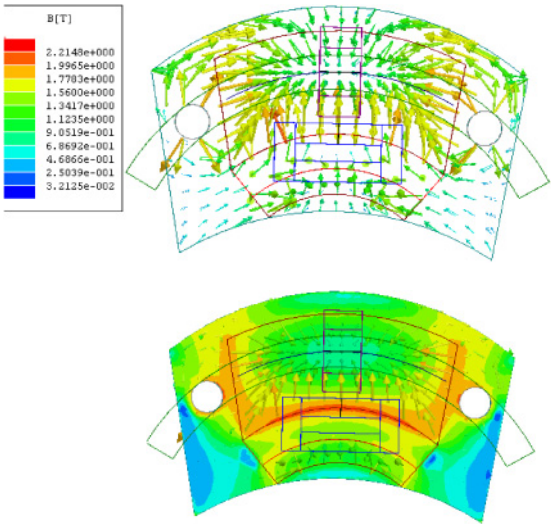


**Fig. 10.** (Color online) 3D EM model and magnetic flux lines on cross-sectional view of base yoke.

driving force generated by the VCM is discussed. We prefer the magnetic circuit design for suppressing mode vibration. The four, hollow, rectangular tracking and focusing coils are attached to the moving seesaw arm. Three fan-shaped NdFeB magnets are combined with the base yoke. The yoke, the focusing coil, the tracking coils, and the magnets form a magnetic circuit. Lorentz force is generated in this magnetic circuit and drives the moving part in the focusing and tracking directions. As shown in Fig. 9, there is a ring yoke to obtain higher sensitivity by making a more efficient magnetic circuit around the tracking coils. The ring yoke is magnetized by the biggest fan-shaped magnet and enclosed in the direction of the magnetic line. Owing to the ring yoke constraint, the magnetic flux is uniform in the tracking coil and the magnetic field intensity is strengthened to 0.505 T. The peak of this vibration mode depends on the magnetic flux density distribution. Therefore, a uniform magnetic flux distribution in the tracking direction improves the dynamic characteristics of the actuator.

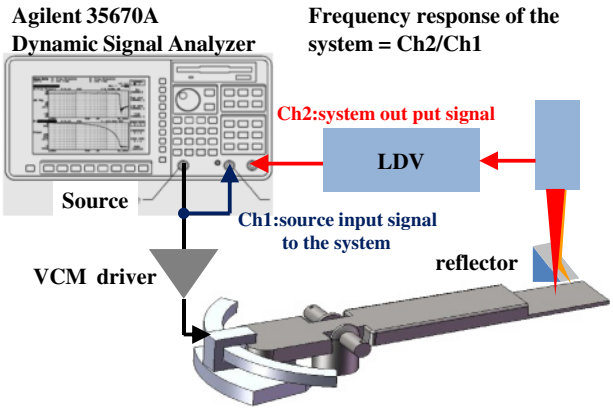


**Fig. 11.** (Color online) Dynamic response experimental apparatus.

## 4. Fabrication and Experiments

The new seesaw rotary VCM actuator is shown in Figs. 5 and 8. The initial seesaw arm is constructed of an aluminum alloy to suppress the magnetic effect between the EM circuits. The sleeve in the middle of the seesaw arm was made from stainless steel, the yokes were made from cold rolled carbon steel sheets and strip (SPCC), which is a grade of commercial steel referenced as the Japanese standard, and the fan-shaped magnets consists of NdFeB. Instead of an integrated pickup, a ballast mockup with the same mass was used for the dynamic tests. The performance of the fabricated actuator was evaluated in the tracking and focusing directions because they were sufficient to check the initial dynamic characteristics. In the experiment for dynamic characteristics measurement shown in Fig. 11, the relative displacement of the fabricated actuator is the only measurable output and is measured using a laser Doppler vibrometer (LDV). A dynamic signal analyzer (DSA; Agilent 35670A) is used to measure the frequency response of the VCM actuator. The DSA also records both input and output signals of the time domain response.

The design concepts are aimed at achieving high performance and miniaturization. The seesaw arm selection of the clamp modes is critical for the performance of the device. This strongly affects the two main parameters of the actuator, the mechanical strength and the servo bandwidth. The design features are shown in Fig. 12. The fabricated seesaw actuator frequency response from VCM input to lens displacement is dominated by the rigid body mode in the low-frequency range and the structural vibration modes in the high-frequency range. The DC sensitivity is 0.194 mm/V, and the first resonance frequency occurs at approximately 22 Hz in the tracking direction. The second resonance frequency occurs at 3 kHz. In more detail, it is found that the first resonance frequency occurs at 35 Hz in the focusing direction and the second resonance frequency occurs at 3.1 kHz. The cantilever mode response is close to that of the ANSYS simulation.

In the experiment for magnetic characteristics measurement, we used a digital Gauss meter (F.W. BELL 5180) to measure the magnetic flux density between the ring yoke and the MSMA magnets. From the experimental results shown in Fig. 13, the starting value of the normal flux density in the air gap is 0.38 T, higher than the initial value, and converges


© 2010 The Japan Society of Applied Physics

Person-to-person distribution (up to 10 persons) by the author only. Not permitted for publication for institutional repositories or on personal Web sites.



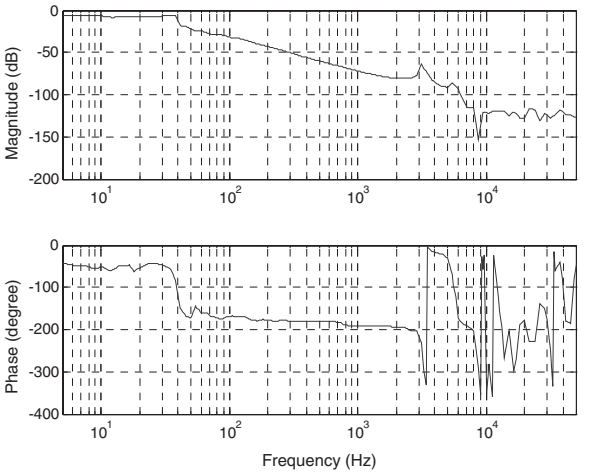


(a)

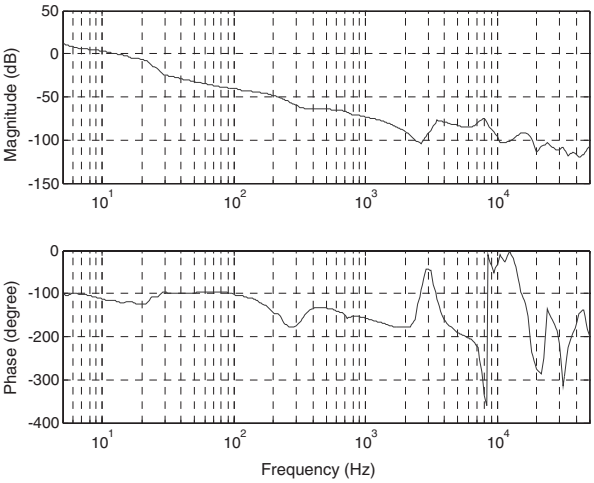


(b)

**Fig. 12.** Measured seesaw actuator frequency responses: (a) focusing direction and (b) tracking direction.

to 0.505 T. Comparing the measured data with the simulation value, the variation of the flux density is within 1%, which coincides with the VCM specifications. This high flux density provides a source of generating a larger actuating force and can make the system move faster. We expect that this magnetic circuit design process can be applied to the design phases of other types of VCM, such as holographic optical storage systems.

## 5. Optimized Design of the Seesaw Mechanism

As shown in Fig. 12, the previous fabricated seesaw actuator did not have a sufficient dynamic characteristic of the second resonance frequency in the focusing direction. To apply this actuator to optical storage devices, the sufficient bandwidth should be over 3 kHz, which is the actuator bandwidth. Moreover, the actuator components are simplified to reduce the inaccuracies in the manufacturing and assembly processes. As shown in the previous conception, redesigning of the coupling pins to clamp down the seesaw arm motion cannot sufficiently satisfy the first bending mode frequency for focusing. The total mass of moving parts should be counterbalanced in the fulcrum of the seesaw arm, and the stress energy distribution should be decreased to maintain

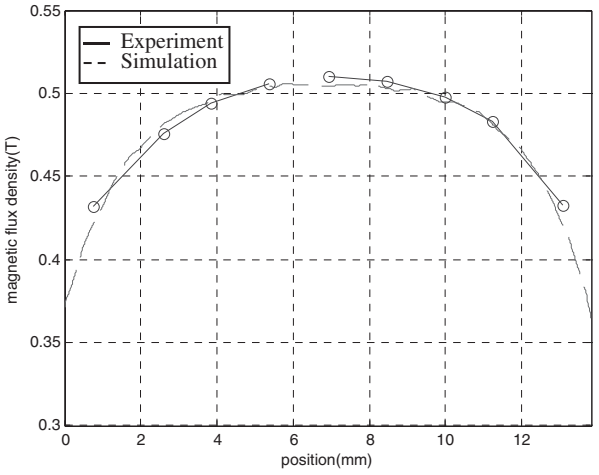


**Fig. 13.** Magnetic flux density results contrast.

high sensitivity. To determine the design variables, the optimal functions can be represented as follows:

Optimal function 1:

$$\max|\text{second resonance frequency (Hz)}| = \max\sum|\text{first bending mode frequency}| \quad (1)$$

Optimal function 2:

$$\min|\text{mass of actuator moving part (g)}| = \min\sum|\text{arm} + \text{coil} + \text{bearing} + \text{pickup head} + \text{pin}| \quad (2)$$

Optimal function 3:

The product of magnetic flux densities $\boldsymbol{b}$ obtained in each node and the current applied to the voice coil make the driving forces $\boldsymbol{f}$ affect each node of the coil. The force component for each nodes of the coil can be obtained by

$$\boldsymbol{f} = nl(\boldsymbol{i} \times \boldsymbol{b}) \quad (3)$$

where $n$ is the number of voice coil turns in each element, $l$ is the effective length of the coil in the each element, $\boldsymbol{i}$ is the driven current applied to the coil, and $\boldsymbol{b}$ is the magnetic flux density at each node.

The focusing magnetic force is spread over the focusing coil and the tracking magnetic force is distributed in the tracking coil. The magnetic distribution represents the vertical and horizontal dimensions of the focusing and tracking coils. The resultant force exerted on the coil is expressed by

$$\min|\text{driven force } \boldsymbol{F}| = \min\sum|\boldsymbol{f}|. \quad (4)$$

The seesaw actuator with the new focusing mechanism is shown in Fig. 14; this assembly consists of two matched reinforced alloy components above the pin and seesaw arm, and is inserted horizontally into the $1.5 \times 3 \times 1\,\text{mm}^3$ pivot bearing with the steel pin accurately embedded in the lateral pinholes of the seesaw arm. The matching surfaces of the pin and seesaw arm are adhesive without protrusion, and the main bearing bore of the rotary base is machined for the use of precision main bearing inserts. An unsettled pin may result in eccentric rotation and wear of the seesaw arm pivot bearing. The reliability of the pivot bearing is evaluated by considering the reliability of its elements and their connections. Low abrasion rotation provides a more robust and


© 2010 The Japan Society of Applied Physics

Person-to-person distribution (up to 10 persons) by the author only. Not permitted for publication for institutional repositories or on personal Web sites.



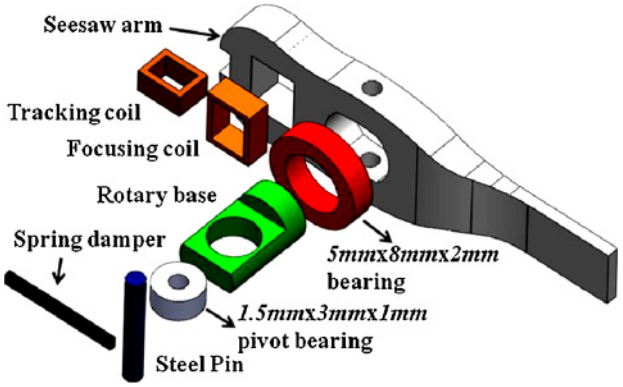


**Fig. 14.** (Color online) Exploding design of seesaw type actuator.

accurate focusing motion than the original design; however, to ensure the optical system stability and the balance between optimal theory and practice, a spring damper is used to connect the focusing coil to the rotary base, and maintains the static balance required to provide both the stability and optimal functionality of the seesaw actuator—it also withstands static and dynamic loads in the motion. Since the driving action and the damping reaction are oppositely directed, the spring damper has an opposite damping force when the seesaw arm is focusing. These two contributions inside the damper tend to cancel each other. Therefore, the suggested focusing actuator has an accurate focusing motion and lower power consumption than previous designs.

The moving parts of the actuator are deformed in various ways, including shearing, twisting, and bending. Such deformations, or changes in shape, are known as strains. If the stresses and strains in the seesaw arm and rotary base are too large, they will possibly make the VCM actuator break. Hence, we rely on strength-of-materials data and modify the seesaw configuration by specifying suitable forms for the various parts of the seesaw actuator. To maintain the high sensitivity of the seesaw actuator while reducing the mass of the swing arm, parts that are closely connected to the strain energy distribution of a considered mode should be reinforced. To restrain the stress concentration, the stress distribution of the seesaw-type actuator was calculated by finite element analysis (FEA), as shown in Fig. 15. The range of stress magnitude distribution of the optimum design $0.0002-0.1204\,\mathrm{N/mm^2}$, is better than that of the initial design of $0-3.3103\,\mathrm{N/mm^2}$.

We measure the dynamic characteristics to confirm the advantage of the optimum VCM structure shown in Fig. 16. Figure 17 shows the measured transfer function of the new design. The resonance frequency of the tracking response is improved from 3 to 5.5 kHz and the crossover frequency is beyond 5 kHz. The high stiffness and low inertia are important design issues in the swing arm for the low magnitudes of vibration modes and the wide bandwidth of the tracking servo. Precisely, the primary focusing resonant peak appears at 3.75 kHz, accompanied by a phase change of over 180°; other resonant peaks are observed above 4 kHz. A low-frequency resonance peak was also observed at 26 Hz in the focusing direction, and considered to be related to the load beam bending. The resonant vibration modes were measured using a LDV. The primary resonant mode at 3.75 kHz was recognized as a local vibration of the

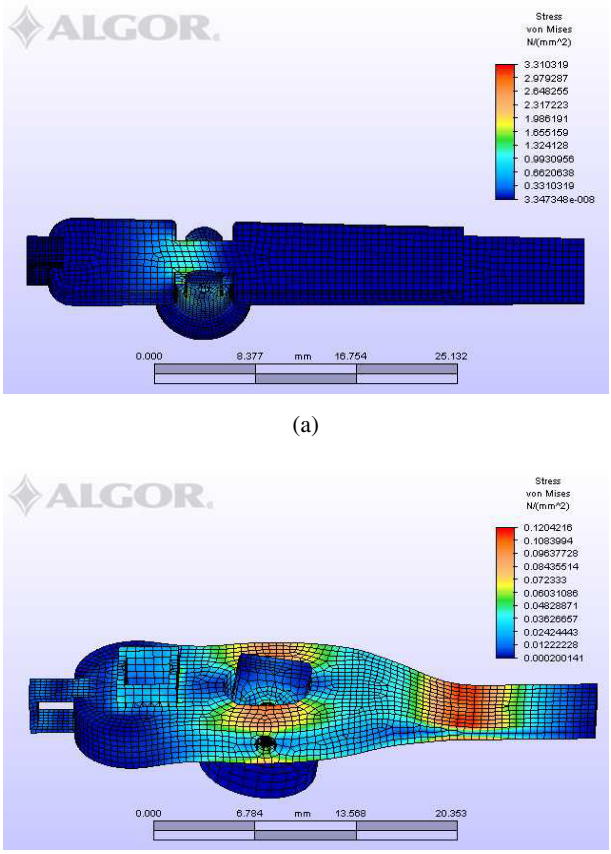


**Fig. 15.** (Color online) Stress distribution of new seesaw type actuator: (a) the initial design of the seesaw swing arm, and (b) the optimum design of the seesaw swing arm.

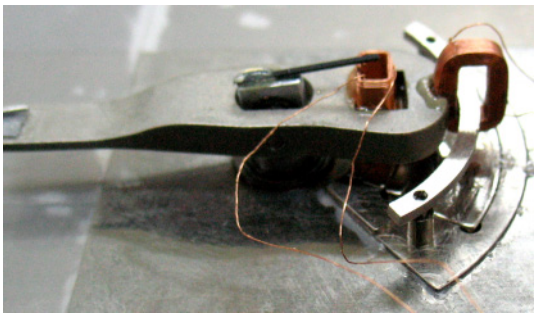

**Fig. 16.** (Color online) Overall structure view of the optimum-design seesaw swing arm actuator.

optimum structure. Above 50 kHz, some local vibration modes of the fabricated structure appeared. Below 10 kHz, the bending and torsion modes of the seesaw arm were observed. As shown in Table III, compared with the initial design, the cantilever mode frequency did not contain significant variations, but the first bending mode frequency was enhanced by 20% while the seesaw actuator was focusing—the coil resistance and the magnet volume were not degraded. Therefore, we achieved a VCM design with a large operation bandwidth. Moreover, we manufactured the new designed actuator and confirmed its performance. The optimal seesaw actuator not only achieves the required specifications of the tracking servo bandwidth but also strengthen the joint of the mechanism.


© 2010 The Japan Society of Applied Physics

Person-to-person distribution (up to 10 persons) by the author only. Not permitted for publication for institutional repositories or on personal Web sites.



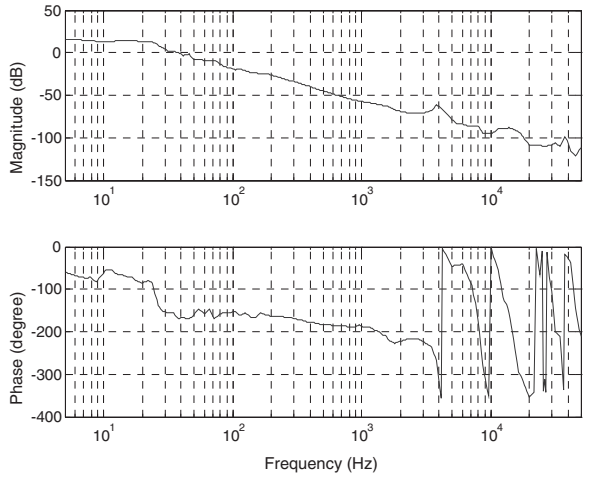


(a)

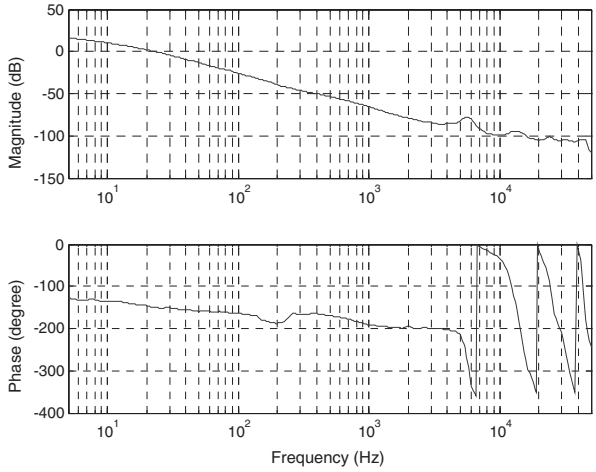


(b)

**Fig. 17.** The measured response of optimum-design seesaw actuator: (a) focusing direction and (b) tracking direction.

To achieve a highly concentrated flux, the magnets tend to be closer to the restrained yokes. If the magnets become denser, compared with the thickness of the yoke, the yoke will be saturated and become impermeable. Since the flux cannot be confined effectively even though the magnets become more packed, enhancing the magnetic forces of the MSMA is not a good solution. During the developmental process, the mechanical design of adjusting the rotary base altitude and diminishing the ring yoke cross section went through many modifications to increase the magnetic flux density. As shown in Table IV and Fig. 18, a VCM adopting additional electromagnetic integration generates denser magnetic flux, and can produce more $X$-directional actuation force from 0.049

**Table III.** Comparison of initial and optimum designed actuators.

| Item | Tuned | Optimized | Improvement (%) |
|---|---|---|---|
| Total mass (g) | 1.87 | 0.96 | −51 |
| Pickup (mg) | 500 | 500 | |
| Focusing coil: | 100 turns | 0.5 Ω | |
| Generate force (N/V) | 0.045017 | 0.045312 | 0.6 |
| Tracking coil: | 150 turns | 0.8 Ω | |
| Generate force (N/V) | 0.049165 | 0.050609 | 2 |
| Focusing direction | | | |
| 1st mode (Hz) | 35 | 26 | −25 |
| 2nd mode (Hz) | 3124 | 3750 | 20 |

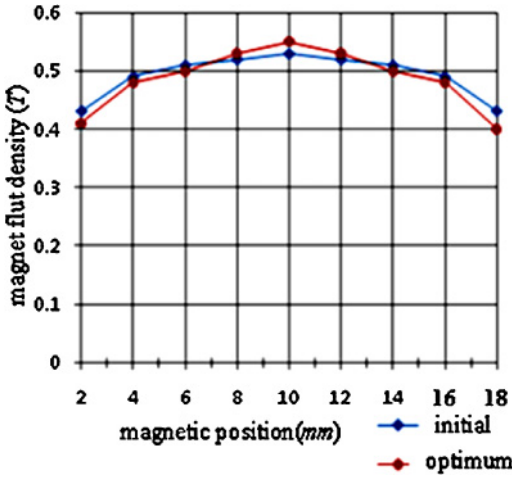


**Fig. 18.** (Color online) Comparison of magnetic flux density between initial design and optimum design.

**Table IV.** Voice coil driven force comparison.

(a) Magnetic force in tracking direction

| Initial design (Tracking coil) | | | | Optimum design (Tracking coil) | | | |
|---|---|---|---|---|---|---|---|
| Main section | | All section | | Main section | | All section | |
| $F(x)$: | 0.04878 | $F(x)$: | 0.04878 | $F(x)$: | 0.052907 | $F(x)$: | 0.050906 |
| $F(y)$: | $-3.3026 \times 10^{-5}$ | $F(y)$: | $-3.3026 \times 10^{-5}$ | $F(y)$: | $-5.8452 \times 10^{-5}$ | $F(y)$: | $7.1682 \times 10^{-5}$ |
| $F(z)$: | 0.00014818 | $F(z)$: | 0.00014818 | $F(z)$: | 0.00018064 | $F(z)$: | $2.9609 \times 10^{-5}$ |
| Mag($F$): | 0.04878 | Mag($F$): | 0.04878 | Mag($F$): | 0.052907 | Mag($F$): | 0.050906 |

(b) Magnetic force in focusing direction

| Initial design (Focusing coil) | | | | Optimum design (Focusing coil) | | | |
|---|---|---|---|---|---|---|---|
| Main section | | All section | | Main section | | All section | |
| $F(x)$: | $6.656 \times 10^{-6}$ | $F(x)$: | $-8.1775 \times 10^{-5}$ | $F(x)$: | $3.9222 \times 10^{-5}$ | $F(x)$: | $-5.2111 \times 10^{-5}$ |
| $F(y)$: | 0.0033259 | $F(y)$: | 0.012047 | $F(y)$: | 0.0037169 | $F(y)$: | 0.012361 |
| $F(z)$: | 0.027565 | $F(z)$: | 0.045017 | $F(z)$: | 0.02763 | $F(z)$: | 0.045312 |
| Mag($F$): | 0.027765 | Mag($F$): | 0.046601 | Mag($F$): | 0.02811 | Mag($F$): | 0.046967 |



© 2010 The Japan Society of Applied Physics

Person-to-person distribution (up to 10 persons) by the author only. Not permitted for publication for institutional repositories or on personal Web sites.



to 0.051 N in the tracking direction, and 0.045 to 0.0453 N in the focusing direction. In addition, the force or the flux density in the magnetic loop becomes more uniform than for the original design without an increase in the actuator size, which means that the modified seesaw arm actuator can be controlled easily using linear control laws as well.

## 6. Conclusions

In this work, the effect of voice coil driving force on the VCM actuator was studied to improve its dynamic characteristic. A new seesaw-type actuator with a MSMA circuit was proposed and fabricated for a micro-ODD. FE analysis verified the actual mechanical characteristics of the actuator system. The performance of the seesaw arm was tuned using EM analysis to reduce the magnitude of the natural frequency vibrations. An optimum design of the swing arm for application in a micro-ODD system is carried out with the original design. The magnetic flux density and the actuating force are obtained and the usefulness of the new VCM is investigated through several experiments and simulations. The improved model had a second resonance frequency in the focusing direction that is 20% greater than the original design, and its parts had a total mass that is 51% less than those of the initial model. It is known that the VCM with a MSMA can produce more force than that conventional VCM. For an actuator producing an equivalent force, the ring yoke with the MSMA can be more compact.

## Acknowledgements

This work was supported by TDPA project 95-EC-17-A-07-S1-011, MOEA, and NSC project NSC 96-2221-E-009-149, Taiwan, ROC.

1) M. G. Song, J. H. Woo, N. C. Park, J. Yoo, Y. P. Park, and K. S. Park: Microsyst. Technol. **16** (2009) 205.
2) D. J. Lee, J. H. Woo, S. U. Kim, J. S. Oh, J. H. Yoo, N. C. Park, Y. P. Park, T. Shimano, and S. Nakamura: Jpn. J. Appl. Phys. **46** (2007) 3715.
3) D. Ju Lee, S. June Park, J. Oh, N. C. Park, Y. P. Park, and H. S. Jung: Jpn. J. Appl. Phys. **45** (2006) 1124.
4) J. Jeong and D. G. Gweon: Jpn. J. Appl. Phys. **46** (2007) 2912.
5) D. L. Blankenbeckler, B. W. Bell, Jr., K. Ramadurai, and R. L. Mahajani: Jpn. J. Appl. Phys. **45** (2006) 1181.
6) E. J. Hong, D. W. Kim, N. C. Park, H. S. Yang, Y. P. Park, and S. K. Kim: Microsyst. Technol. **11** (2005) 1085.
7) E. J. Hong, W. S. Oh, N. C. Park, H. S. Yang, and Y. P. Park: Microsyst. Technol. **11** (2005) 506.
8) J. R. Edwards: IEEE Trans. Magn. **35** (1999) 863.
9) M. Sgwa and K. Aruga: IEEE Trans. Magn. **35** (1999) 868.
10) H. F. Shih, C. L. Chang, K. J. Lee, and C. S. Chang: IEEE Trans. Magn. **41** (2005) 1058.
11) D. L. Blankenbeckler, D. H. Davies, W. W. A. Dunford, B. W. Bell, Jr., and R. H. Hamer: Jpn. J. Appl. Phys. **43** (2004) 4896.
12) Y. Chiu, H. F. Shih, J. C. Chiou, S. T. Cheng, K. Y. Hung, F. G. Tseng, and W. Fang: IEEE Trans. Magn. **45** (2009) 2194.
13) D. L. Blankenbeckler, B. W. Bell, Jr., D. H. Davies, and L. W. Lee: Proc. SPIE **5380** (2004) 171.
14) F. Gao, F. F. Yap, and Y. Yan: IEEE Trans. Magn. **41** (2005) 744.
15) H. S. Lee, Y. H. Kim, T. Y. Hwang, and C. S. Kim: IEEE Trans. Magn. **41** (2005) 774.
16) D. J. Lee, G. W. Jung, N. C. Park, H. S. Yang, Y. P. Park, B. Y. Song, W. I. Cho, P. Y. Seong, and K. H. Lee: Jpn. J. Appl. Phys. **44** (2005) 3373.
17) J. Jeong, M. G. Lee, J. H. Lee, H. K. Yoon, and D. G. Gweon: Jpn. J. Appl. Phys. **43** (2004) 1398.
18) M. G. Lee, J. Jeong, and D. G. Gweon: Jpn. J. Appl. Phys. **42** (2003) 3394.
19) C. Kaido: IEEE Transl. J. Magn. Jpn. **9** (1994) No. 6, 110.


© 2010 The Japan Society of Applied Physics